Organic Geochemistry 217 (2026) 105192

Contents lists available at ScienceDirect

Organic Geochemistry

journal homepage: www.elsevier.com/locate/orggeochem

# Plant wax D/H fractionation in modern plants from the Falkland Islands

Mark D. Peaple [a,*], Gordon N. Inglis [b], Paul D.M. Hughes [a], Zoë Thomas [a]

[a] School of Geography and Environmental Science, University of Southampton, University Road, Southampton SO17 1BJ, UK
[b] School of Ocean and Earth Science, University of Southampton, European Way, Southampton SO14 3ZH, UK

ARTICLE INFO

Associate Editor: Nikolai Pedentchouk

*Keywords:*
Plant wax
Falkland Islands
Hydrogen isotope
Isotopic fractionation

ABSTRACT

The hydrogen isotopic composition ($\delta^2H$) of plant waxes is a powerful tool for reconstructing past precipitation, yet its accuracy relies on constraining the apparent fractionation ($\varepsilon$) between plants and source water ($\varepsilon_{wax/water}$). While regional information on *n*-alkanes exists in the Falkland Islands, values for *n*-alkanoic acids remain unconstrained, despite the latter often being more abundant in sedimentary archives. To address this, we analysed paired *n*-alkanes and *n*-alkanoic acids from modern plant species in the Falkland Islands. We present a regional dataset for n-alkanoic acids (n = 9), finding a mean fractionation ($\varepsilon_{acid/precip}$) of –147 ± 22‰. This is broadly consistent with co-occurring *n*-alkanes (–137 ± 20‰), validating the use of *n*-alkanoic acids as a complementary proxy. Comparing our *n*-alkane data with previous studies reveals a ~ 28‰ offset in ($\varepsilon_{alkane/precip}$), which we attribute to distinct plant communities and year-to-year variability in precipitation $\delta^2H$ affecting source water. We also assess the influence of high-biomass species on landscape-scale ($\varepsilon_{alkane/precip}$). Our new abundance-weighted mean fractionation factor for the combined *n*-alkane dataset (–129‰) is statistically indistinguishable from the unweighted community mean (–121‰) and demonstrates that high-biomass species do not skew the landscape-scale signal, providing confidence in using $\delta^2H$ for quantitative paleoclimate reconstruction in the Falkland Islands.

## 1. Introduction

The Falkland Islands (51.7°S) are situated directly within the mean-annual path of the Southern Hemisphere Westerlies (SHW), an atmospheric system that profoundly influences regional precipitation, temperature, and Southern Ocean dynamics (Toggweiler et al., 2006). As a result, sedimentary plant wax isotope records from the islands serve as a highly sensitive archive for reconstructing past shifts in the position and strength of the westerlies (Spoth et al., 2023). Understanding these shifts is crucial, as the westerlies are a primary control on regional precipitation patterns and strongly influence Southern Ocean dynamics, ocean carbon flux, and regional cryosphere mass balance. Accurate interpretation of these archives, however, requires a robust understanding of the distribution and natural variability of the hydrogen isotopic composition of modern local plant waxes ($\delta^2H_{wax}$).

$\delta^2H_{wax}$ is a widely applied proxy for reconstructing the $\delta^2H$ of past precipitation (Sachse et al., 2012). However, accurately applying this proxy requires constraining the apparent fractionation ($\varepsilon_{wax/precip}$) that occurs between source water and the *n*-alkyl lipids synthesised by plants (Smith and Freeman, 2006; Hou et al., 2007). This fractionation varies between plant species due to differences in their biosynthetic pathways (Smith and Freeman, 2006; Hou et al., 2007), meaning the net landscape-integrated $\varepsilon_{wax/precip}$ is determined by the composition of the plant community. Subsequently, changes in vegetation through time can introduce large uncertainty into palaeoclimate reconstructions (Feakins, 2013).

In the Falkland Islands, foundational work by Corcoran et al. (2022) characterised the $\varepsilon_{wax/precip}$ of long-chain *n*-alkanes across 10 plant species, demonstrating that the regional mean fractionation value (–109 ± 18‰) is broadly consistent with global averages (McFarlin et al., 2019). Building on this work, we expand the analysis to include n-alkanoic acids. This addition is valuable as *n*-alkanoic acids are often more abundant than *n*-alkanes in sedimentary archives (Andersson and Meyers, 2012; Wu et al., 2019), but remain entirely unconstrained in this climate-sensitive region.

Building on this initial research, our study refines the regional $\varepsilon_{wax/precip}$. We present the first hydrogen isotope fractionation data for *n*-alkanoic acids from the Falkland Islands plant community (including graminoids, ferns, woody shrubs, forbs, and mosses) and expand the existing *n*-alkane dataset. By integrating these results, we provide a

* Corresponding author.
*E-mail address:* M.D.Peaple@soton.ac.uk (M.D. Peaple).

https://doi.org/10.1016/j.orggeochem.2026.105192
Received 28 October 2025; Received in revised form 3 March 2026; Accepted 15 March 2026
Available online 20 March 2026

community-integrated $\varepsilon_{wax/precip}$ that quantifies natural precipitation variability and includes a broader range of plant species, thereby strengthening the foundation for future palaeoclimate studies in the region.

## 2. Methods

Modern plant leaves were collected from six peatland sites across the Falkland Islands: Canopus Hill, Kingsford Valley, Penguin Cove, Plaza Creek, Pond Mountain, and Weddell Island (March 2024; Fig. 1a). To ensure sufficient material for analysis, approximately 5–10 leaves were sampled per individual plant, depending on leaf size, targeting a wet tissue mass of ~1 g. A detailed list of the specific plant species collected and site coordinates is provided in the publicly available data deposition (Peaple, 2025). Total lipid extracts (TLEs) were obtained from freeze-dried plant material (mean = 0.37 g) via sonication in dichloromethane:methanol (DCM:MeOH, 9:1, v/v). The TLEs were separated into neutral and acid fractions using aminopropyl ($NH_2$) column chromatography. The neutral fraction was eluted with 2:1 DCM:isopropanol, and the acid fraction was subsequently eluted with 4% formic acid in DCM. The neutral fraction was further purified by eluting with hexane through a silica gel column to isolate *n*-alkanes, which were treated with activated copper to remove sulphur. The acid fraction was methylated using 95:5 MeOH:HCl (70 °C, 12 h) to convert *n*-alkanoic acids to their corresponding fatty acid methyl esters (FAMEs). Compound quantification was performed on a Thermo Trace 1310 GC-FID. The Carbon Preference Index (CPI) and Average Chain Length (ACL) were calculated to characterize lipid distributions:

$$CPI = \frac{2[C_n]}{[C_{n-1}] + [C_{n+1}]} \quad (1)$$

$$ACL = \frac{\Sigma(n[C_n])}{\Sigma[C_n]} \quad (2)$$

where $C_n$ refers to the *n*-alkane or *n*-alkanoic acid of length *n* (for $C_{23}$ to $C_{31}$ *n*-alkanes, and $C_{22}$ to $C_{32}$ *n*-alkanoic acids).

Stable hydrogen and carbon isotopic compositions ($\delta^2H$ and $\delta^{13}C$) of individual *n*-alkanes and FAMEs were measured at the University of Southampton using a Thermo Trace 1310 GC coupled to a Delta V Plus Isotope Ratio Mass Spectrometer (IRMS). Analyses for $\delta^2H$ used a pyrolysis furnace (1400 °C), while $\delta^{13}C$ analyses used a combustion furnace (1000 °C). Data were normalized to the VSMOW and VPDB scales, respectively, using an external *n*-alkane standard (A6 mix, A. Schimmelmann) run 5 times a day. Average RMS errors on the standard were <2‰ for $\delta^2H$ and <0.2‰ for $\delta^{13}C$. The $H_3^+$ factor was monitored daily, with a mean value of 3.33 ppm/mV. To account for the added methyl group, we apply a mass balance correction (Polissar and D'Andrea, 2014) to the measured *n*-alkanoic acid methyl esters. The correction is based on the isotopic values from a methylated phthalic acid standard supplied by A. Schimmelmann (Lee et al., 2017).

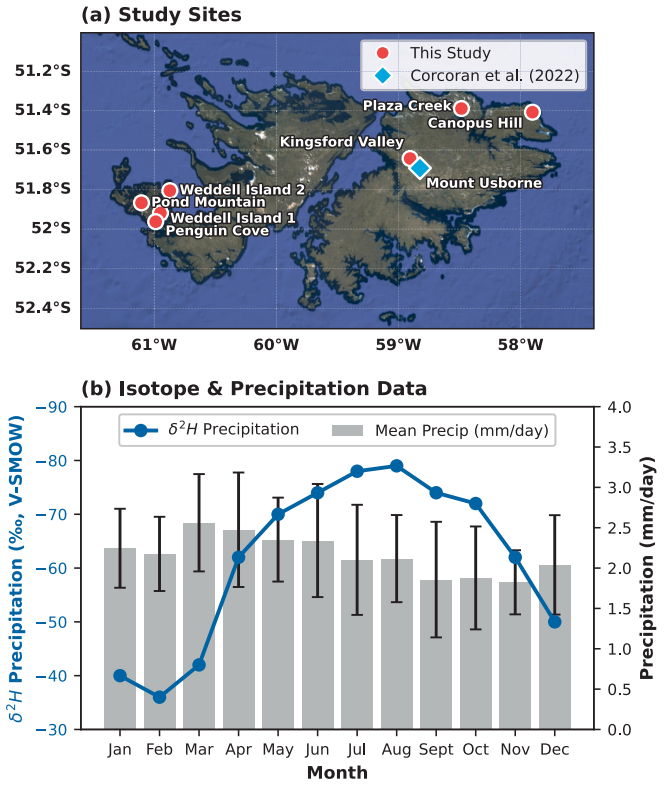


**Fig. 1.** Study area and regional climatology. (a) Satellite map of the Falkland Islands showing the location of sampling sites. Red circles indicate sites sampled in this study, while the cyan diamond indicates the reference site (Mount Usborne) from Corcoran et al. (2022). (b) Seasonal variation in precipitation and isotopes (Bowen, 2025). Grey bars display mean monthly precipitation (mm/day) with error bars representing one standard deviation. The blue line shows the annual cycle of precipitation $\delta^2H$ (‰ V-SMOW), plotted on an inverted y-axis. (For interpretation of the references to colour in this figure legend, the reader is referred to the web version of this article.)

## 3. Results and discussion

### 3.1. Plant wax distributions

Two general patterns were identified in the dataset regarding *n*-alkyl lipid distribution (Fig. 2). First, *n*-alkanes were generally more abundant than *n*-alkanoic acids, with a mean alkane-to-acid ratio of 14.5. An exception was the fern *Blechnum penna-marina*, which displayed an *n*-alkanoic acid-dominant ratio (alkane-to-acid ratio: 0.01), consistent with previous observations for fern species (Lee et al., 2017). Second, total *n*-alkane concentrations were highly variable, ranging from <20 μg/g in the fern to ~25,000 μg/g in the graminoid *Festuca magellanica*.

Graminoids exhibited the highest concentrations of *n*-alkyl waxes. The highest values were found in *Festuca magellanica* (~25,000 μg/g), *Festuca contracta* (3494 μg/g), and *Luzula alopecurus* (3236 μg/g). This group also had high ACL for both *n*-alkanes (mean = 28.7) and *n*-alkanoic acids (mean = 27.7), and high CPI values (*n*-alkane mean = 61.5, *n*-alkanoic acid mean = 26.5). An exception within this group was *Marsippospermum grandiflorum*, which had a lower *n*-alkane ACL of 26.8. Forbs and woody shrubs showed intermediate and variable wax concentrations and distributions. Forbs had average *n*-alkane concentrations of 222 (±331) μg/g and ACL values that were similar to graminoids (mean *n*-alkane ACL = 27.6; *n*-alkanoic acid = ACL 27.1). Mosses had lower concentrations of *n*-alkanes (mean *n*-alkane concentration = 33.5 μg/g, mean alkanoic acid concentration 11.0 μg/g). Mosses also showed the lowest ACL values for alkanoic acids (mean = 24.4), which is consistent with peat datasets (Naafs et al., 2019). The mean alkane ACL of Sphagnum magellanicum (24.3) also fits this trend, but *Sphagnum fimbriatum* exhibits a higher alkane ACL of 27.9. This divergence between *n*-alkane and *n*-alkanoic acid ACL patterns in some *Sphagnum* species has been previously observed (Baas et al., 2000) and is likely driven by a combination of environmental and/or genetic factors (Bingham et al., 2010). As summarised in Fig. 3, the aggregated molecular metrics highlight the distinct central tendencies and variability within each plant functional type. For instance, the distributions demonstrate the exceptionally wide range in CPI among graminoids (*n*-alkane CPI: 7.3 to 185.5; *n*-alkanoic acid CPI: 8.3 to 26.5) compared with the more constrained variance seen in woody shrubs (*n*-alkane CPI: 10.2 to 39.5) and mosses (*n*-alkane CPI: 23.3 to 46.9).

The results show that while functional plant groups generally display distinct chemotaxonomic patterns, specific taxa diverge from group

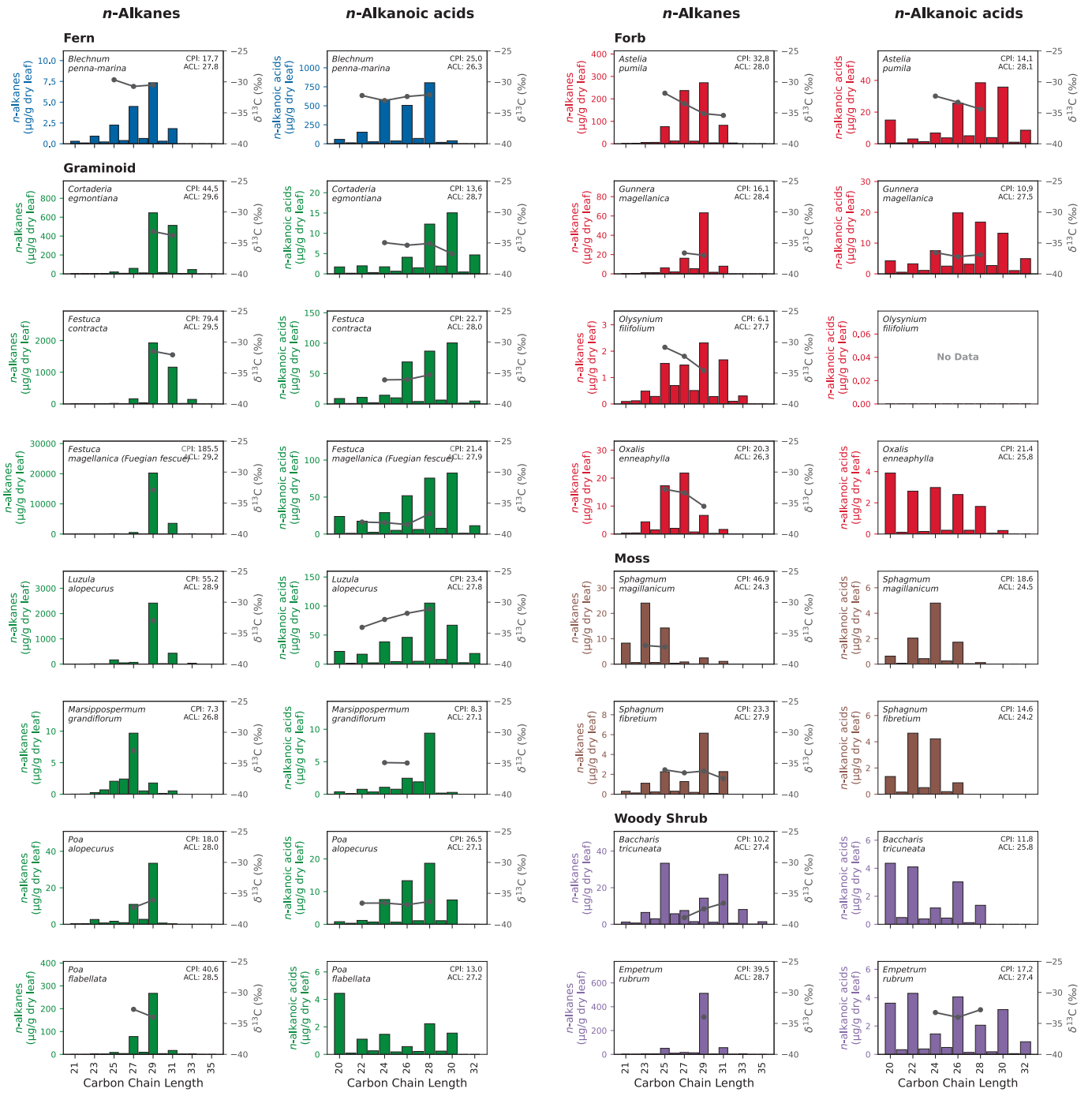


**Fig. 2.** Distributions and carbon isotopic composition ($\delta^{13}C$) of leaf wax *n*-alkyl lipids in modern plants from the Falkland Islands. The panels are organised by plant functional type: graminoids, ferns, woody shrubs, forbs, and mosses. For each species, paired histograms display the distributions of (left) *n*-alkanes and (right) *n*-alkanoic acids. Bars represent lipid concentrations (µg/g dry leaf mass), with colours corresponding to plant functional types. Note that the y-axis scales for concentration vary between species to highlight distribution patterns. Grey lines with markers indicate compound-specific carbon isotope values ($\delta^{13}C$, ‰) where data were available. The inset boxes display the Carbon Preference Index (CPI) and Average Chain Length (ACL) calculated for the respective homologue series. X-axis represent the carbon chain length. Empty plots indicate where a compound class was not detected or was below quantification limits.

means. Notably, *Marsipposperrmum* and *S. fimbriatum* display outlier ACL values in their *n*-alkane distributions that could lead to misclassification if used in isolation. However, these deviations are often class specific. For instance, while *S. fimbriatum* exhibits a high 'vascular-like' *n*-alkane ACL, it retains the characteristically low *n*-alkanoic acid ACL of mosses. Consequently, a multi-proxy approach is essential; by cross-validating *n*-alkanoic acid and *n*-alkane fingerprints, we can resolve these specific ambiguities and constrain the biological source more accurately than with a single lipid class.

### 3.2. Carbon Isotope Composition and Chemotaxonomic Implications

The $\delta^{13}C$ of the analysed *n*-alkanes and *n*-alkanoic acids ranges from –38.9‰ to –29.7‰ (Fig. 2). These values fall entirely within the range characteristic of plants utilising the C3 photosynthetic pathway (–41.4‰ to –28.6‰, 2σ range from Liu and An, 2020) confirming the absence of C4 vegetation in the cool, maritime climate of the Falkland Islands. While there is overlap in $\delta^{13}C$ values across plant functional types, we observe minor systematic differences; for instance, the fern

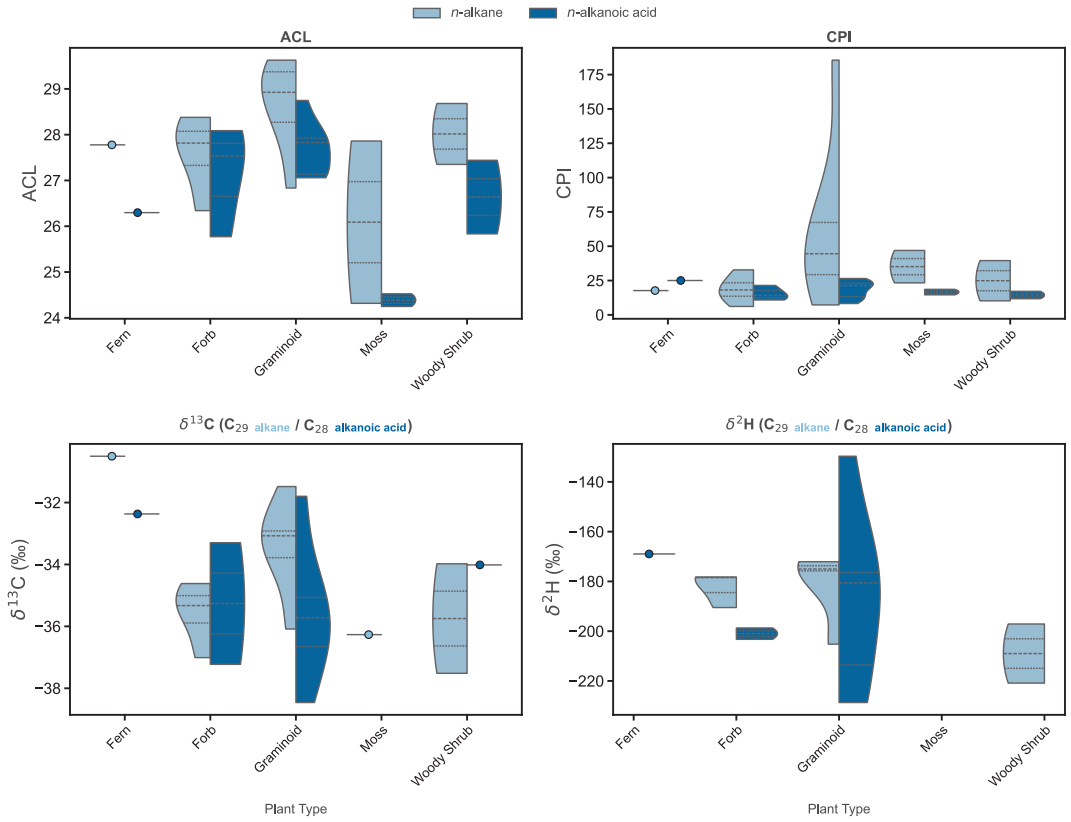


**Fig. 3.** Molecular and stable isotopic distributions of leaf wax lipids (*n*-alkanes and *n*-alkanoic acids) across five major plant growth forms. The top panels illustrate the structural metrics of the lipid arrays, showing (Top Left) Average Chain Length (ACL) and (Top Right) Carbon Preference Index (CPI). The bottom panels display the stable isotopic compositions, specifically comparing the $C_{29alkane}$ *and the* $C_{28acid}$ (Bottom Left) $\delta^{13}C$ (‰) and (Bottom Right) $\delta^{2}H$ (‰). Split violin plots represent the probability density of the data, with *n*-alkanes depicted in light blue (left half) and *n*-alkanoic acids in dark blue (right half). Interior horizontal lines within the violins denote data quartiles. Solid circular markers indicate singleton data points (n = 1) for a specific plant type and lipid class where density distributions could not be calculated. (For interpretation of the references to colour in this figure legend, the reader is referred to the web version of this article.)

*Blechnum penna-marina* exhibits notably positive $\delta^{13}C$ values (mean *n*-alkane $\delta^{13}C$ = –30.3‰) compared with the more negative values observed in graminoids such as *Festuca magellanica* (–32.9‰) and woody shrubs like *Empetrum rubrum* (–34.0‰). These offsets are consistent with previous regional observations (Corcoran et al., 2022) and likely reflect differences in water-use efficiency and stomatal conductance inherent to these growth forms. When grouped by functional type (Fig. 3), the $\delta^{13}C$ distributions clearly visualize these systematic offsets, highlighting the distinctly positive isotopic space occupied by ferns ($\delta^{13}C_{C29alkane}$ = –30.5‰; $\delta^{13}C_{C28acid}$ = –32.4‰) compared with the broader, more negative ranges of graminoids ($\delta^{13}C_{C29alkane}$: –36.1‰ to –31.5‰; $\delta^{13}C_{C28acid}$: –38.5‰ to –31.8‰) and forbs ($\delta^{13}C_{C29alkane}$: –37.0‰ to –34.6‰).

Our dataset reveals that wax concentrations vary by over three orders of magnitude across the landscape. For example, the graminoid *Festuca magellanica* is a hyper-producer of *n*-alkanes (~20,000–25,000 μg/g), whereas *Blechnum* ferns produce negligible amounts (~5–20 μg/g; Fig. 2). Consequently, even if ferns are present in the catchment, their relatively positive $\delta^{13}C$ and $\delta^{2}H$ signals are likely to be dominated by the high-concentration input from graminoids and shrubs.

### 3.3. Plant Wax Hydrogen Isotopic Fractionation

The measured hydrogen isotopic compositions ($\delta^{2}H_{wax}$) of the dominant long-chain lipids show considerable ranges across plant species and functional type (Fig. 3). For *n*-alkanoic acids, $\delta^{2}H$ values of the $C_{28}$ homolog range from –229‰ to –129‰. For *n*-alkanes, the $C_{29}$ homolog values range from –221‰ to –172‰. Grouped by functional type (Fig. 3), these $\delta^{2}H$ values reveal distinct clusterings, such as the highly negative values observed in woody shrubs ($\delta^{2}H_{C29alkane}$: –220.9‰ to –197.1‰) compared with the broader ranges seen in graminoids ($\delta^{2}H_{C29alkane}$: –205.2‰ to –172.1‰; $\delta^{2}H_{C28acid}$: –228.7‰ to –129.7‰). However, these ranges show significant overlap and likely reflect the influence of plant-specific biosynthetic effects (Sachse et al., 2012; Sessions, 2016).

We quantified the apparent hydrogen isotope fractionation ($\varepsilon_{wax/precip}$) between leaf wax lipids ($C_{28}$ *n*-alkanoic acid and $C_{29}$ *n*-alkane) and precipitation for modern plants from the Falkland Islands. The $\varepsilon_{wax/precip}$ value was calculated using the formula:

$$\varepsilon_{wax/precip} = [(\delta^{2}H_{wax} + 1000) / (\delta^{2}H_{precip} + 1000) - 1] \times 1000 \quad (3)$$

To constrain $\varepsilon_{wax/precip}$ we used long-term mean annual $\delta^{2}H_{precip}$ values for our sampling sites, obtained from the Online Isotopes in Precipitation Calculator (OIPC). Although distinct local values were applied at each sampling location, the modelled precipitation isotopes were spatially consistent across the study area, yielding a mean of –57.5 ± 3.1‰ (Bowen and Revenaugh, 2003; Bowen, 2025; IAEA, WMO, 2025). While early growth-season precipitation can strongly influence lipid isotopic composition in well-drained soils (e.g., Saishree et al., 2024), peat bogs can exhibit substantial hydrological buffering and extended water residence times (Morris and Waddington, 2011). Given the lack of site-specific constraints on seasonal water pools and species-specific rooting depths, we adopted mean annual $\delta^{2}H_{precip}$ as a conservative, time-integrated baseline for calculating fractionation factors, consistent with previous regional studies (Corcoran et al., 2022).

The mean $\varepsilon_{wax/precip}$ for *n*-alkanoic acids was –147‰, which is lower than that of the *n*-alkanes (–137‰), although a Kolmogorov-Smirnov test indicates the underlying distributions of the two compound

classes are not statistically distinct. While similar differences between $\varepsilon_{acid/precip}$ and $\varepsilon_{alkane/precip}$ have been observed in global core top compilations (McFarlin et al., 2019) and between individual plant species (Feakins et al., 2016; Freimuth et al., 2017) we note that the central tendencies could simply be skewed due to low sample numbers. Nonetheless, the general consistency between the distributions supports their use as complementary proxies.

A critical consideration for palaeoclimate studies is whether the sedimentary archive accurately reflects the diverse plant community or is biased by high-biomass species. Our concentration data (Fig. 2) reveal that wax production varies by over three orders of magnitude, with "hyper-producers" like Festuca magellanica (~25,000 μg/g) potentially dominating the input flux. To test this, we compared the unweighted mean fractionation of our combined *n*-alkane dataset (–121 ± 22‰) against an abundance-weighted mean. The abundance-weighted mean was calculated by weighting each species' average fractionation value proportionally to its total measured *n*-alkane concentration. The resulting weighted value (–129 ± 13‰) is statistically indistinguishable from the unweighted mean ($p > 0.05$). This convergence suggests that the high-production graminoids possess fractionation factors representative of the broader community. Consequently, despite the large spread in individual species values, the central tendency of the proxy remains stable regardless of whether the sedimentary input is driven by high biodiversity or high biomass production. We note that this assumes the species dominating landscape biomass have been adequately characterised (inclusive of this study and Corcoran et al., 2022). While an uncharacterized, rare 'hyper-producer' with anomalous fractionation could theoretically exist, its low landscape abundance would limit its total net flux (which is governed by landscape coverage, leaf turnover, and ablatability), preventing it from skewing the integrated sedimentary signal.

When these datasets are combined with those of Corcoran et al. (2022), the integrated fractionation factor captures a more representative range of the region's natural variability (Fig. 4). Viewed in isolation, the single-year studies show a significant offset; our mean $\varepsilon_{wax/precip}$ value is ~28‰ lower than that reported by Corcoran et al. (2022). To assess if this offset was driven by taxonomic differences, we compared species common to both studies. We observed substantial intraspecific variability; for example, the widespread shrub *Empetrum rubrum* yielded a $C_{29}$ $\delta^2H$ of –221‰ in our dataset, compared with a mean of –176‰ reported by Corcoran et al. (2022). Conversely, the forb *Astelia pumila* showed closer agreement (–178‰ vs. –192‰). The persistence of these offsets within identical species indicates that the broader discrepancy likely reflects the combined influence of inter-annual climate shifts affecting source water $\delta^2H$, local microclimate effects, and distinct plant communities. Examining this variability by plant type (Fig. 4) reveals that forbs, graminoids, and woody shrubs have broadly similar unweighted means (–115‰, –132‰, and –124‰, respectively), while ferns are notably more positive (–92‰). This indicates that unless there is a substantial shift in the proportion of fern-derived waxes, changes in the dominant plant community are unlikely to significantly bias palaeoclimate reconstructions of $\delta^2H_{precip}$ in this region.

## 4. Conclusions

This study presents the first regional hydrogen isotope fractionation data for *n*-alkanoic acids in the Falkland Islands. The mean fractionation for *n*-alkanoic acids ($\varepsilon_{acid/precip}$ = –147 ± 22‰) is broadly consistent with that of co-occurring *n*-alkanes, supporting the utility of acids as a complementary proxy for paleohydrological reconstructions. We assessed the potential for bias driven by vegetation structure by comparing abundance-weighted and unweighted fractionation values for the combined *n*-alkane dataset. The abundance-weighted mean (–129 ± 13‰) is statistically indistinguishable from the unweighted community mean (–121 ± 22‰). This agreement suggests that, despite *n*-alkyl lipid concentrations varying by orders of magnitude across the landscape, the integrated isotopic signal exported to sedimentary archives (e.g., peats) is not disproportionately skewed by high-biomass species such as *Festuca magellanica*. The integrated isotopic signal incorporates a wider range of spatial and inter-annual variability than single-season studies, providing a refined baseline for converting sedimentary $\delta^2H_{wax}$ records into precipitation isotopes and providing confidence in using $\delta^2H$ for quantitative paleoclimate reconstruction in the Falkland Islands. Future work extending this dataset across seasonal

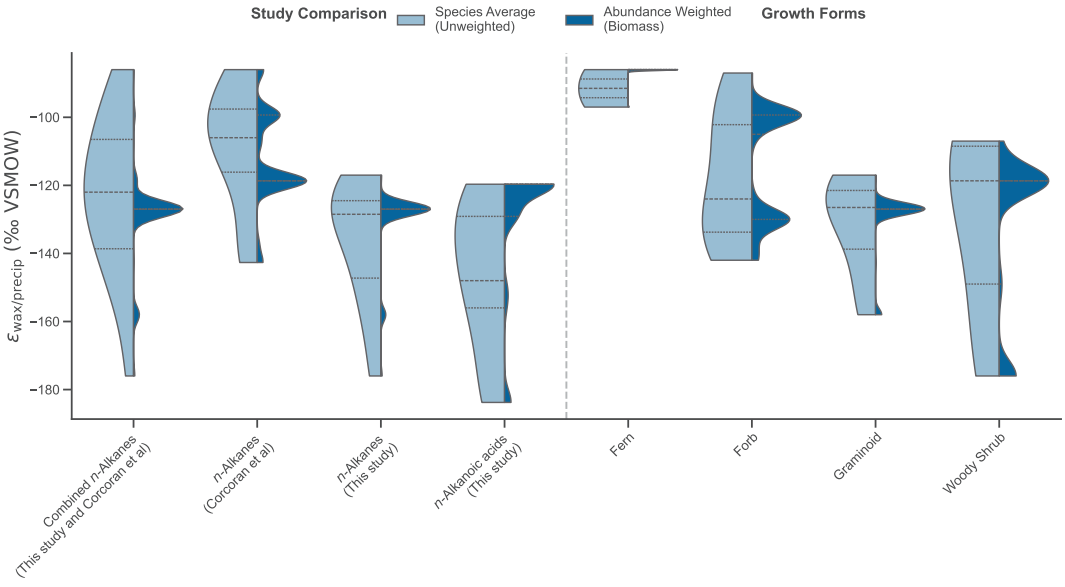


**Fig. 4.** Comparison of unweighted and abundance-weighted biosynthetic hydrogen isotope fractionation ($\varepsilon_{wax/precip}$) values for Falkland Islands plant waxes. Split violin plots display the kernel density estimation of the data: the left half (light blue) represents the distribution of unique species means (unweighted, where each species counts as one observation), while the right half (dark blue) represents the distribution weighted by the relative abundance of *n*-alkanes or n-alkanoic acids per species. Horizontal lines within the violins mark the 25th, 50th (median), and 75th percentiles. Plant data combines results from this study and Corcoran et al. (2022), encompassing *n*-alkanes $C_{21}$-$C_{33}$ and *n*-alkanoic acids $C_{22}$-$C_{32}$. This comparison demonstrates how high-biomass species (e.g., Festuca magellanica) influence the aggregate isotopic signal compared with a simple species average. Values are reported in per mil (‰) relative to VSMOW. (For interpretation of the references to colour in this figure legend, the reader is referred to the web version of this article.)

cycles would further constrain these environmental controls.

## CRediT authorship contribution statement

**Mark D. Peaple:** Writing – review & editing, Writing – original draft, Visualization, Project administration, Methodology, Investigation, Formal analysis, Data curation, Conceptualization. **Gordon N. Inglis:** Writing – review & editing, Supervision, Funding acquisition, Conceptualization. **Paul D.M. Hughes:** Writing – review & editing, Validation, Investigation. **Zoë Thomas:** Writing – review & editing, Supervision, Project administration, Funding acquisition, Conceptualization.

## Declaration of competing interest

The authors declare that they have no known competing financial interests or personal relationships that could have appeared to influence the work reported in this paper.

## Acknowledgments

This work was funded by a UKRI FLF award to Z.T. (MR/Y016351/1). GNI was supported by a Royal Society Dorothy Hodgkin Fellowship (DHF/R1/191178). We are grateful to the South Atlantic Environmental Research Institute (SAERI) for facilitating fieldwork, and to the many landowners who kindly provided access permissions. We also thank Dmitri Mauquoy for providing *Sphagnum* samples and the reviewers for their comments, which have significantly strengthened the manuscript.

## Data availability

Data presented in this study are publicly available at Zenodo (Peaple, 2025).

## References

Andersson, R.A., Meyers, P.A., 2012. Effect of climate change on delivery and degradation of lipid biomarkers in a Holocene peat sequence in the eastern European Russian Arctic. Organic Geochemistry 53, 63–72. https://doi.org/10.1016/j.orggeochem.2012.05.002.

Baas, M., Pancost, R., van Geel, B., Sinninghe Damsté, J.S., 2000. A comparative study of lipids in Sphagnum species. Organic Geochemistry 31, 535–541. https://doi.org/10.1016/S0146-6380(00)00037-1.

Bingham, E.M., McClymont, E.L., Väliranta, M., Mauquoy, D., Roberts, Z., Chambers, F. M., Pancost, R.D., Evershed, R.P., 2010. Conservative composition of n-alkane biomarkers in Sphagnum species: Implications for palaeoclimate reconstruction in ombrotrophic peat bogs. Organic Geochemistry 41, 214–220. https://doi.org/10.1016/j.orggeochem.2009.06.010.

Bowen, G.J., Revenaugh, J., 2003. Interpolating the isotopic composition of modern meteoric precipitation. Water Resources Research 39, 2003WR002086. https://doi.org/10.1029/2003WR002086.

Bowen, G., 2025. OIPC: The online isotopes in precipitation calculator, version 3.1 [WWW Document]. URL http://www.waterisotopes.org.

Corcoran, M.C., Diefendorf, A.F., Lowell, T.V., Hall, B.L., Spoth, M.M., Schartman, A., Brickle, P., 2022. Hydrogen and carbon isotope fractionation in modern plant wax n-alkanes from the Falkland Islands. Organic Geochemistry 166, 104404. https://doi.org/10.1016/j.orggeochem.2022.104404.

Feakins, S.J., 2013. Pollen-corrected leaf wax D/H reconstructions of northeast African hydrological changes during the late Miocene. Palaeogeography, Palaeoclimatology, Palaeoecology 374, 62–71. https://doi.org/10.1016/J.PALAEO.2013.01.004.

Feakins, S.J., Bentley, L.P., Salinas, N., Shenkin, A., Blonder, B., Goldsmith, G.R., Ponton, C., Arvin, L.J., Wu, M.S., Peters, T., West, A.J., Martin, R.E., Enquist, B.J., Asner, G.P., Malhi, Y., 2016. Plant leaf wax biomarkers capture gradients in hydrogen isotopes of precipitation from the Andes and Amazon. Geochimica et Cosmochimica Acta 182, 155–172. https://doi.org/10.1016/j.gca.2016.03.018.

Freimuth, E.J., Diefendorf, A.F., Lowell, T.V., 2017. Hydrogen isotopes of *n*-alkanes and *n*-alkanoic acids as tracers of precipitation in a temperate forest and implications for paleorecords. Geochimica et Cosmochimica Acta 206, 166–183. https://doi.org/10.1016/J.GCA.2017.02.027.

Hou, J., D'Andrea, W.J., MacDonald, D., Huang, Y., 2007. Hydrogen isotopic variability in leaf waxes among terrestrial and aquatic plants around Blood Pond, Massachusetts (USA). Organic Geochemistry 38, 977–984. https://doi.org/10.1016/j.orggeochem.2006.12.009.

IAEA, WMO, 2025. Global Network of Isotopes in Precipitation, The GNIP Database [WWW Document]. URL https://nucleus.iaea.org/wiser.

Lee, H., Feakins, S.J., Lu, Z., Schimmelmann, A., Sessions, A.L., Tierney, J.E., Williams, T. J., 2017. Comparison of three methods for the methylation of aliphatic and aromatic compounds. Rapid Communications in Mass Spectrometry 31, 1633–1640. https://doi.org/10.1002/rcm.7947.

Liu, J., An, Z., 2020. Leaf wax *n*-alkane carbon isotope values vary among major terrestrial plant groups: different responses to precipitation amount and temperature, and implications for paleoenvironmental reconstruction. Earth-Science Reviews 202, 103081. https://doi.org/10.1016/j.earscirev.2020.103081.

McFarlin, J.M., Axford, Y., Masterson, A.L., Osburn, M.R., 2019. Calibration of modern sedimentary $\delta^2$H plant wax-water relationships in Greenland lakes. Quaternary Science Reviews 225, 105978. https://doi.org/10.1016/j.quascirev.2019.105978.

Morris, P.J., Waddington, J., 2011. Groundwater residence time distributions in peatlands: implications for peat decomposition and accumulation. Water Resources Research 47, W02511. https://doi.org/10.1029/2010WR009492.

Naafs, B.D.A., Inglis, G.N., Blewett, J., McClymont, E.L., Lauretano, V., Xie, S., Evershed, R.P., Pancost, R.D., 2019. The potential of biomarker proxies to trace climate, vegetation, and biogeochemical processes in peat: a review. Global and Planetary Change 179, 57–79. https://doi.org/10.1016/j.gloplacha.2019.05.006.

Peaple, M., 2025. Modern plant wax distributions and hydrogen isotope compositions from the Falkland Islands. 10.5281/ZENODO.17456274.

Polissar, P.J., D'Andrea, W.J., 2014. Uncertainty in paleohydrologic reconstructions from molecular δD values. Geochimica et Cosmochimica Acta 129, 146–156. https://doi.org/10.1016/j.gca.2013.12.021.

Sachse, D., Billault, I., Bowen, G.J., Chikaraishi, Y., Dawson, T.E., Feakins, S.J., Freeman, K.H., Magill, C.R., McInerney, F.A., van der Meer, M.T.J., Polissar, P., Robins, R.J., Sachs, J.P., Schmidt, H.-L., Sessions, A.L., White, J.W.C., West, J.B., Kahmen, A., 2012. Molecular paleohydrology: interpreting the hydrogen-isotopic composition of lipid biomarkers from photosynthesizing organisms. Annual Review of Earth and Planetary Sciences 40, 221–249. https://doi.org/10.1146/annurev-earth-042711-105535.

Saishree, A., Managave, S., Yadava, M., Devi, S.M., Sanyal, P., 2024. Tropical leaf wax *n*-alkane and *n*-alkanoic acid reflect δD of precipitation during early stages of leaf growth: Insights from an isotope labeling experiment. Paleoceanography and Paleoclimatology 39, e2024PA004899. https://doi.org/10.1029/2024PA004899.

Sessions, A.L., 2016. Factors controlling the deuterium contents of sedimentary hydrocarbons. Organic Geochemistry 96, 43–64. https://doi.org/10.1016/j.orggeochem.2016.02.012.

Smith, F.A., Freeman, K.H., 2006. Influence of physiology and climate on δD of leaf wax *n*-alkanes from $C_3$ and $C_4$ grasses. Geochimica et Cosmochimica Acta 70, 1172–1187. https://doi.org/10.1016/J.GCA.2005.11.006.

Spoth, M., Hall, B., Lowell, T., Diefendorf, A.F., Corcoran, M.C., Brickle, P., 2023. Tracking the southern hemisphere westerlies during and since the last glacial maximum with multiproxy lake records from the Falkland Islands (52°S). Quaternary Science Reviews 311, 108135. https://doi.org/10.1016/j.quascirev.2023.108135.

Toggweiler, J.R., Russell, J.L., Carson, S.R., 2006. Midlatitude westerlies, atmospheric CO2, and climate change during the ice ages. Paleoceanography 21, PA2005. https://doi.org/10.1029/2005PA001154.

Wu, M.S., West, A.J., Feakins, S.J., 2019. Tropical soil profiles reveal the fate of plant wax biomarkers during soil storage. Organic Geochemistry 128, 1–15. https://doi.org/10.1016/j.orggeochem.2018.12.011.